Defect Spectroscopy on Damp-Heat Treated ZnO/CdS/Cu(In,Ga)(S,Se)$_2$/Mo Heterojunction Solar Cells

C. Deibel, V. Dyakonov, and J. Parisi

Department of Energy and Semiconductor Research, Faculty of Physics,
University of Oldenburg, D-26111 Oldenburg, Germany

Reprint requests to Prof. J.P.; E-mail: Parisi@ehf.uni-oldenburg.de.

The changes of defect characteristics induced by accelerated lifetime tests on solar cells of the heterostructure ZnO/CdS/Cu(In,Ga)(S,Se)$_2$/Mo are investigated. Encapsulated modules were shown to be stable against water vapor and oxygen under outdoor conditions, whereas the fill factor and open-circuit voltage of non-encapsulated test cells are reduced after prolonged damp heat treatment in the laboratory, leading to a reduced energy conversion efficiency. We subjected non-encapsulated test cells to extended damp heat exposure at 85 °C ambient temperature and 85% relative humidity for various time periods (6 h, 24 h, 144 h, 294 h, and 438 h). In order to understand the origin of the pronounced changes of the cells, we applied temperature-dependent current-voltage and capacitance-voltage measurements, admittance spectroscopy, and deep-level transient spectroscopy. We observed the presence of electronic defect states which show an increasing activation energy due to damp heat exposure. The corresponding attempt-to-escape frequency and activation energy of these defect states obey the Meyer-Neldel relation. We conclude that the response originates from an energetically continuous distribution of defect states in the vicinity of the CdS/chalcopyrite interface. The increase in activation energy indicates a reduced band bending at the Cu(In,Ga)(S,Se)$_2$ surface. We also observed changes in the bulk defect spectra due to the damp-heat treatment. – PACS: 73.20.hb, 73.61.Le

Key words: Cu(In,Ga)(S,Se)$_2$; Solar Cells; Damp Heat; Defect Spectroscopy.

1. Introduction

Cu(In,Ga)(S,Se)$_2$ based thin film solar cells display relatively high energy conversion efficiencies on laboratory scale devices [1] as well as large area modules [2–4]. These heterostructures basically consist of a transparent front contact (highly doped ZnO), a buffer layer (usually CdS), the Cu(In,Ga)(S,Se)$_2$ chalcopyrite absorber itself, and a back contact (e.g., Mo). Considering that these layers mostly are of polycrystalline nature and contain more than ten different constituents, it seems to be surprising that this cell concept shows such high performance and reproducibility. The physical understanding of the underlying principles of electronic transport and morphological properties, however, always remains a step behind the technological invention [5].

An important key prerequisite for the success of solar cells as powerful sources of renewable energy is their long-term stability under outdoor conditions. In particular, the influence of water vapor and oxygen on the charge transport properties of the heterostructure cells is the focus of our paper. Oxygen-related phenomena have been discussed in the literature for more than a decade [6], and extensive work covering oxygenation [7] and related topics [8] is available. The impact of water vapor on the cell characteristics goes beyond the magnitude of the influence of oxygen [9], even though both effects are closely related to each other.

Encapsulated Cu(In,Ga)(S,Se)$_2$ based thin-film modules have been demonstrated to perpetuate their performance over many years under various environmental conditions [9]. In order to understand the potential power losses developing over the course of decades, standardized accelerated lifetime tests assist the investigation to be performed within a few weeks. The acceleration factor of these stress tests relative to a field test is presently still unknown; it would be needed for a reliable extrapolation of the module lifetime based on stress examination results. For that purpose we look for a better understanding of stress-test induced changes in the device. The most severe part of the well-established IEC 1215 (ISPRA) test is an exposure of the cells under investigation to 1000 h of damp heat (DH) treat-

ment at a temperature of 85 °C and relative humidity of 85%. Improved technology and encapsulation procedures led to reduction of degradation effects, thus modules fabricated to date passed the accelerated lifetime tests [9 – 11]. Non-encapsulated CuInSe$_2$-based solar cells, however, show losses in the fill factor and open-circuit voltage after exposure to the DH test, whereas the short-circuit current remains almost unaffected.

Changes of the transport properties of CuInSe$_2$ based thin-film solar cells due to exposure to DH have recently been investigated with regard to modifications in the window [9, 12, 13] and absorber layer [14 – 18]. So far, the impact of stress tests on the back contact of the solar cells has been described only qualitatively [12, 13]. A fraction of the DH induced changes is reversible under illumination (referred to as light soaking). Such metastability most likely originates from the absorber layer [9]. In this context (also concerning the differences of DH exposure to oxygenation [7]), it should be mentioned that the effect of dry air annealing (85 °C, 2000 h) on the electronic properties is much smaller than that of DH exposure [9].

Admittance spectroscopy [19] and deep-level transient spectroscopy (DLTS) [20] have proven to be important aids in the process of understanding the charge carrier transport in CuInSe$_2$ based heterostructure devices and Schottky contacts [21, 22]. Investigation of defect states in semiconductors allows for monitoring the electronic changes induced by chemical or morphological modifications due to oxygenation and exposure to DH.

In the present study we analyze the influence of accelerated lifetime tests on non-encapsulated ZnO/CdS/Cu(In,Ga)(S,Se)$_2$/Mo heterostructure solar cells and Cr/Cu(In,Ga)(S,Se)$_2$/Mo Schottky contacts, focussing on the electronic properties of the Cu(In,Ga)(S,Se)$_2$ absorber and the interface between window and absorber. In Sect. 2, the experimental methods used for electrical characterization are briefly described. The experimental results of current-voltage and capacitance-voltage measurements, admittance spectroscopy, and DLTS concerning the modifications of the electronic properties due to DH exposure are presented in Sect. 3. Calculations of the possible loss factors present in DH treated Cu(In,Ga)(S,Se)$_2$ solar cells were performed using the device simulation programme SCAPS [23] (Sect. 4). Section 5 is divided into parts discussing our findings for each layer of the heterostructure. Finally, Sect. 6 gives a summary and the conclusions of our paper.
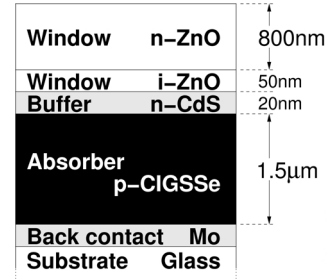

Fig. 1. Schematic diagram of the cross-sectional structure of our ZnO/CdS/Cu(In,Ga)(S,Se)$_2$/Mo heterojunction samples. Note that CIGSSe is a conventional abbreviation of Cu(In,Ga)(S,Se)$_2$.

2. Experimental Methods

The samples investigated consist of non-encapsulated ZnO/CdS/Cu(In,Ga)(S,Se)$_2$/Mo heterojunction solar cells (see Fig. 1) and Cr/Cu(In,Ga)(S,Se)$_2$ Schottky contacts. The chalcopyrite absorber thin film was fabricated via a two-step process based on rapid thermal processing (RTP) of stacked elemental layers. A 20 nm thick layer of CdS was deposited on top of the Cu(In,Ga)(S,Se)$_2$ film in a chemical bath. The transparent front contact, a ZnO layer of about 800 nm thickness, is deposited by r.f. and d.c. sputtering. The preparation process is described elsewhere in detail [2]. The Schottky devices were produced by deposition of a 50 nm thick Cr film on top of the Cu(In,Ga)(S,Se)$_2$ surface, followed by a 200 nm thick Au layer for mechanical protection [18]. Accelerated lifetime testing was performed under the standardized DH conditions at 85 °C ambient temperature and 85% relative humidity for various time periods (24 h, 144 h, 294 h, and 438 h). For different sets of samples, the processing sequence was interrupted for a DH treatment after the RTP, the CdS bath deposition, or the i-ZnO sputter procedure, respectively. After 6 h or 24 h under exposure to heat and humidity, the cell process (or the deposition of the Schottky contact) was continued. Instead of DH treatment, one set of samples was annealed in dry air atmosphere (85 °C, 24 h) after RTP.

We have characterized the modification of the solar cell parameters of our samples using current-voltage measurements under AM 1.5 (solar spectrum) illumination at 25 °C. Admittance spectroscopy measurements were performed using a Solartron 1260 impedance analyzer, operating with an alternating voltage of 30 mV amplitude at frequencies in the range be-

tween 1 Hz and 1 MHz. In order to look at the interface properties of our samples, we have changed the external voltage from zero to reverse bias. Capacitance-voltage measurements were carried out at $T = 90$ K and a frequency of 100 kHz. DLTS was done applying two spectrometers, a Semitrap 82E apparatus (using also the reverse DLTS (R-DLTS) mode [24]) and a custom-built transient DLTS based on a Boonton 7200 capacitance meter (response time about 120 µs). The Semitrap spectrometer applies a fixed alternating voltage amplitude of 100 mV, for the transient-DLTS setup we chose 50 mV. In both cases, the sampling frequency for measuring the transients of the sample capacitance is 1 MHz. The transients are evaluated with exponential fits or the Laplace transform method [25]. Temperature-dependent analysis was performed using a helium closed-cycle cryostat.

The characterization of defect states with admittance spectroscopy and DLTS is based on the determination of the temperature-dependent emission rates of the trap states, where the activation energy and capture cross-section of the traps can be evaluated from. The thermal emission rate e_t satisfies the equation

$$e_t = \sigma_t v_{th} N_{C/V} \exp\left(\frac{\Delta E}{kT}\right), \qquad (1)$$

where σ_t denotes the capture cross-section, v_{th} the thermal velocity of the charge carriers, $N_{C/V}$ the effective density of states, ΔE the activation energy of the defect level, k the Boltzmann constant, and T the absolute temperature. Both, $N_{C/V}$ and ΔE are related to the valence or conduction band, depending on whether electron or hole emission is dominant, respectively.

For determination of the two characteristic parameters of a defect state, namely, the activation energy and the capture cross-section, the temperature dependence of both, the prefactor and the exponent of the emission rate, has to be considered. The thermal velocity is proportional to $T^{1/2}$, whereas $N_{C/V} \propto T^{3/2}$. Details about the origin of defect states in Cu(In,Ga)(S,Se)₂ are still mostly unknown. Calculations studying the defect physics of CuInSe₂ related compounds are mainly concerned with the formation and activation energies of defects and defect complexes [26]. Since, to our knowledge, the temperature dependence of the capture cross-section of deep states in the above material has not been studied yet, we assume the capture cross-section to be temperature independent, in order to simplify our analysis. We follow the custom of researchers
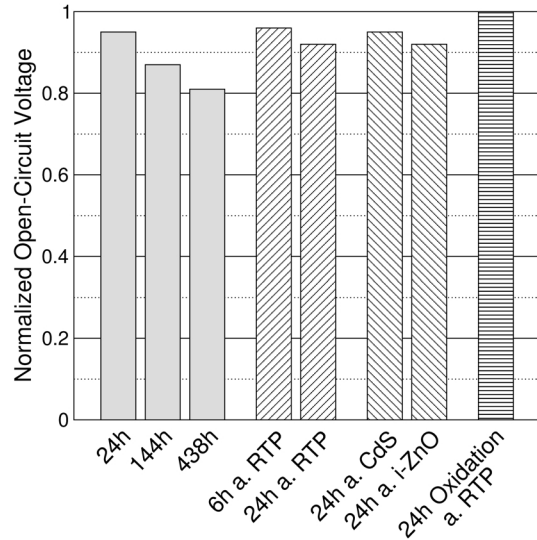

Fig. 2. Histogram of the normalized open-circuit voltage of different sets of DH treated samples. For some sets of samples, the processing sequence was interrupted for a DH treatment after the deposition of a certain layer. The cell process was continued afterwards. The corresponding samples are denoted as, e.g., 6 h a. RTP, meaning 6 h of DH exposure after deposition of the absorber layer. Instead of DH treatment, one set of samples was annealed in dry air atmosphere (85 °C, 24 h) after RTP.

in that material class [17, 23, 27] and neglect the degeneracy and the entropy factor [28]. These simplifications imply that the values of the activation energy determined might be somewhat distorted. Consequently, the temperature-dependent emission rate, being the finger print of the related defect state, is the most reliable quantity for comparing electronically determined defect states with each other.

3. Experimental Results

3.1. Current-Voltage Characteristics

Current-voltage measurements are suitable for macroscopically monitoring changes of the heterojunction charge transport properties. The effect of exposing our non-encapsulated test samples to H_2O vapor manifests in losses in the fill factor and the open-circuit voltage, whereas the short-circuit current remains almost unaffected. Figure 2 exemplarily shows the decrease in the open-circuit voltage after DH testing. We note that the change in open-circuit voltage for samples with DH treated absorbers is very similar to

that of cells that are DH treated after deposition of the CdS buffer or the i-ZnO window layer. The effect of annealing in dry air at 85 °C for 24 h on the electronic properties is fully reversible.

A hysteresis of the current-voltage characteristics at forward bias can only be observed for the DH treated devices when the direction of the voltage sweep is changed, indicating a screening effect which might be connected to charging of deep traps. This effect is also seen in the DH treated Schottky contacts [18]. The current vs. voltage measurements performed before and after DH testing do not indicate the formation of a back-contact barrier (for samples exposed to DH conditions as complete devices), a problem commonly reported for the case of standard CdTe-based solar cells [29].

3.2. Capacitance Spectroscopy

3.2.1. General Observations

The effective doping density of the Cu(In,Ga)(S,Se)$_2$ based heterostructure samples was determined using capacitance-voltage $(C - V)$ measurements. These experiments were performed at 90 K and 100 kHz in order to minimize the influence of deep levels, which then cannot follow the capture-emission process and, thus, do not contribute to the capacitance signal. The slope of the resulting Mott-Schottky plots $(1/C^2$ versus $V)$ clearly shows that the net doping concentration diminishes from 5.5×10^{15} cm^{-3} for as-grown cells to about 2.5×10^{15} cm^{-3} for cells after 144 h of DH treatment [15].

An additional space charge region, e.g., originating from a rectifying (Schottky type) back contact, could neither be observed before nor after exposure of the heterostructure samples to DH conditions.

3.2.2. Interface Defect States

The activation energy of interface defect states was determined by the difference between the quasi-Fermi level and the corresponding energy band. In the case of our heterojunction devices, a defect state at the CdS/Cu(In,Ga)(S,Se)$_2$ interface can be observed using admittance spectroscopy or DLTS in heterostructure cells [15, 27] and Schottky contacts [18]. In the following we will call this interface state β. The origin and magnitude of its activation energy ΔE are indicated in a band diagram of the n-ZnO/i-ZnO/CdS/Cu(In,Ga)(S,Se)$_2$ heterostructure (Fig. 3),
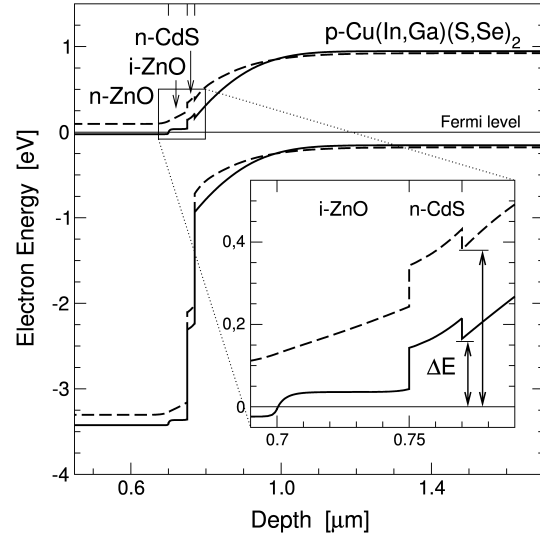

Fig. 3. Band diagram of the n-ZnO/i-ZnO/CdS/Cu(In,Ga)(S,Se)$_2$ heterostructure at thermal equilibrium (with a blow-up focussing on the interfaces at the conduction-band edge). The solid lines represent the conduction and valence band edges of a simulated reference cell. The dashed lines show a case, where the activation energy of a defect state at the CdS/Cu(In,Ga)(S,Se)$_2$ interface is increased due to changes of the interface (i.e., unpinning of the Fermi level) and bulk properties (i.e., increased concentration of a deep acceptor state in the absorber and decreased doping density in both window and absorber). Further details are explained in the text.

describing the position of the Fermi level at the buffer/absorber interface. There are many contributions influencing ΔE, some of which will be discussed later. Cells exposed to the DH environment show a continuous shift of the activation energy and capture cross-section of the interface state β proportional to the exposure time [14, 15]. The main part of this shift proved to be irreversible. A similar behavior was observed after repetitive air annealing for up to two minutes at 240 °C [27].

The common origin of the different instances of the interface state β can be visualized using the Meyer-Neldel relation [30, 31], also called compensation law. It is given by

$$v_0 = v_{00} \exp\left(\frac{\Delta E}{E_c}\right), \qquad (2)$$

where $v_0 = \sigma_t v_{th} N_{C/V}$ means the attempt-to-escape frequency (prefactor of the emission rate, see (1)). v_{00}
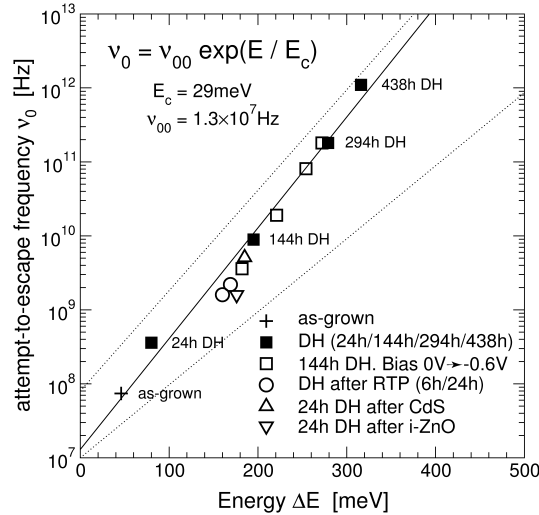
Fig. 4. Attempt-to-escape frequency ν_0 versus activation energy ΔE versus the defect state β following the Meyer-Neldel relation. The solid line corresponds to an exponential fit of the data. The dotted lines are taken from Herberholz et al. [30] for comparison.
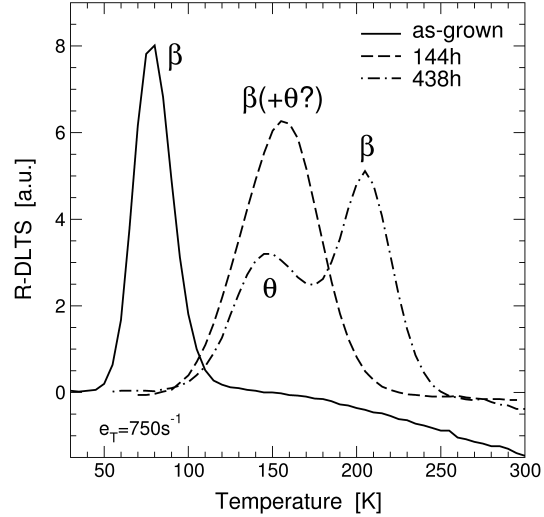
Fig. 5. R-DLTS signal vs. temperature of as-grown and DH-treated (144 h and 438 h) solar cells. The shift of the minority-carrier defect state β and the appearance of the minority-carrier trap θ are due to the DH treatment.

is approximately temperature independent. The characteristic energy E_c leads to the corresponding characteristic temperature $T_c = E_c/k$, defined by the intersection point of all curves in the Arrhenius plot which follow a distinct Meyer-Neldel relation. The interface state β, typically shifting to higher values of the activation energy and capture cross-section with time elapsed under DH conditions, obeys the Meyer-Neldel rule with $E_c = 29$ meV (which is equivalent to $T_c \approx 336$ K) and the prefactor $\nu_{00} = 1.3 \times 10^7$ Hz, as can be seen in Figure 4. We note that the amplitude of the capacitance step related to β decreases proportional to the shift of the activation energy [16].

In DLTS, β was extracted from a minority-carrier signal. Minority carriers usually cannot be injected into Schottky contacts by electrical means, although light pulses are sufficient to do so. However, for Schottky junctions based on n-Si, the observation of minority-carrier traps with DLTS has been reported in case of relatively large barrier heights [32, 33] and moderately large barrier heights [34], using forward bias filling pulses in the latter case. Comparable conditions are given in Cu(In,Ga)(S,Se)$_2$-based heterojunctions, because the observation of a type inversion at the (in-vacuo) Cu(In,Ga)Se$_2$ surface [35] indicates a strong band bending. The minority-carrier state β, being measured with admittance spectroscopy and R-DLTS in

both, heterojunction samples and Schottky contacts, indicates that it is located in the near-surface region of the absorber layer.

As-grown Cu(In,Ga)(S,Se)$_2$-based solar cells usually show Fermi-level pinning at the buffer/absorber interface [15, 23, 27]. The influence of DH treatment on devices that are exposed to the test conditions with the complete heterostructure gives rise to an unpinning of the Fermi level, which manifests in a shift of the interface state β when applying an external bias voltage [15]. The shift of β again complies with the Meyer-Neldel rule (see Figure 4). Devices containing DH treated absorbers, however, still show Fermi-level pinning [15].

A defect state θ was uncovered with the help of R-DLTS after 438 h DH treatment of the whole device, as can be seen in Figure 5. The activation energy was about 140 meV. Since our heterojunction samples do not contain a single-sided abrupt p/n-junction, both edges of the space charge region contribute to the DLTS signal, confounding the determination of the spatial origin of the defect state θ. Taking into account that the shift of β for the above DH treated sample (438 h) indicates a position of the Fermi level of about 300 meV below the conduction-band minimum, the defect state θ would be too shallow to be detected, in case it were located in the absorber layer or at the buffer/absorber interface. Also, θ being a minority-
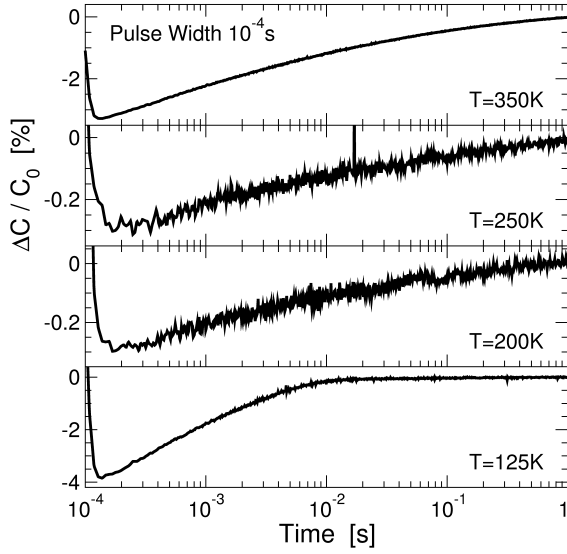
Fig. 6. Capacitance transients of an as-grown Cu(In,Ga)(S,Se)$_2$ heterojunction sample at different temperatures. The 1.5 V filling pulse of 100 μs length was superimposed on a quiescent reverse bias of −1.5 V.

Fig. 7. Capacitance transients of a Cu(In,Ga)(S,Se)$_2$ heterojunction sample exposed to DH conditions for 144 h. The 1.5 V filling pulse of 100 μs length was superimposed on a quiescent reverse bias of −1.5 V.

carrier DLTS signal, it cannot originate from the n-type region, as it could not be observed using capacitance spectroscopy at a position of 140 meV above the valence-band maximum. Thus, the defect state θ presumably is an interface state located at the CdS/ZnO interface or an internal grain boundary.

3.2.3 Bulk Defect States

With the help of capacitance spectroscopy, several defect energy levels located inside the heterostructure devices could be observed. In the following, we will focus on those defect states which seem to be related to the changes of the electrical characteristics of cells exposed to the DH conditions.

A deep defect state, ε, was observed in DLTS spectra recorded before and after DH with conventional and transient DLTS. We observed minority and majority DLTS signals (depending on the amount of injected minority carriers during the filling pulse), both of them resulting in activation energies of about 550 meV. Consequently, we expect the defect state ε to be a recombination center. Its capacitance transient at 350 K for the case without injection pulses can be observed in Fig. 6 for as-grown samples and in Fig. 7 for cells exposed to DH conditions for 144 h. The normalized amplitude $\Delta C/C_0$ of the capacitance transient related to ε
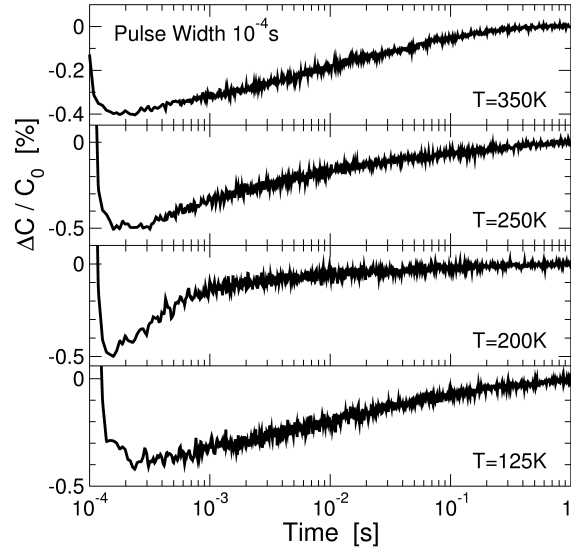
is diminished due to the DH treatment. The determination of the trap concentration is complicated by several circumstances: First, the transient amplitude strongly depends on temperature, indicating the influence of a temperature-dependent capture cross-section or leakage currents (especially for the DH treated device) on the amplitude [36]. Second, the prerequisite for an accurate DLTS analysis, $\Delta C/C_0 \ll 1$ [20], does not hold for the transient of the as-grown sample. Third, the transient does not begin directly after the filling pulse, but is delayed by the response time of the capacitance bridge. Fourth, the transient is non-exponential, and both amplitude and decay strongly depend on the width of the filling pulse. For comparison purposes we used the standard relation for determining the concentration [20], bearing in mind that we only obtain an 'apparent concentration' due to the circumstances mentioned above. For ε at 350 K, we multiplied the normalized amplitude at $t = 130$ μs with the corresponding net doping concentration. For a filling pulse width of 100 μs, we found 2×10^{14} cm^{-3} of ε in the as-grown state and an upper limit of about 10^{13} cm^{-3} for the DH treated sample. For a pulse width of 1 s, the amplitudes were nearly saturated, and we obtained an apparent concentration of 5×10^{14} cm^{-3} for as-grown samples and 2×10^{14} cm^{-3} for samples exposed to DH. A donor-like defect state of similar emission rates, which
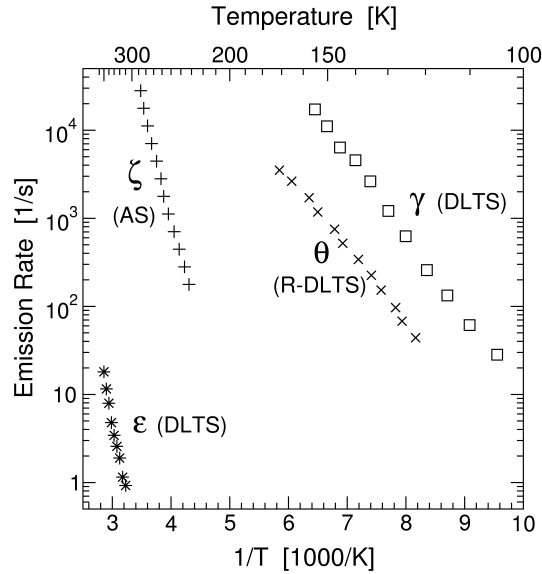
Fig. 8. Arrhenius plot of the four defect states γ (acceptor), ζ (acceptor), θ (minority carrier signal), and ε (recombination center). The abbreviation AS stands for admittance spectroscopy.

shows an increased concentration after DH exposure has been observed by Igalson et al. [17].

We observed an acceptor-like defect state, γ, with conventional and transient DLTS in as-grown samples only. The corresponding capacitance transient at $T = 125$ K is shown in Figure 6. We determined an activation energy of about 160 meV. Similar to ε, the normalized amplitude $\Delta C/C_0$ is diminished due to the DH treatment. An estimation of the concentration, under the same conditions and limitations as described above, yields 2×10^{14} cm^{-3} for as-grown samples at $T = 125$ K in case of both filling pulse widths, 100 μs and 1 s, i.e., the trap is saturated already at the shorter time. We obtained an upper limit for the apparent concentration after the DH treatment of 10^{13} cm^{-3} for a pulse width of 100 μs. For a filling pulse width of 1 s, the amplitude becomes positive: a superposition with the shifted (due to the DH treatment, see Sect. 3.2.2) minority-carrier signal takes place. Such overlapping does not allow for a determination of the concentration, and also puts in question the concentration determined for the short pulse width.

A deep acceptor state, ζ, was detected with admittance spectroscopy and DLTS in as-grown and DH treated Schottky contacts as well as in samples containing absorbers exposed to DH conditions. In samples

DH treated as complete heterostructure, we observed a feature close to the position of ζ with conventional and transient DLTS, but with a relatively small amplitude. The defect state corresponds to the fast decay of the capacitance transient of the DH treated sample at $T = 200$ K, as shown in Figure 7. The apparent concentration of about 10^{13} cm^{-3} is approximately independent of the pulse width. We note that a yet unidentified majority-carrier signal of slightly lower concentration becomes visible for increasing filling pulse widths. The defect state ζ vanishes in the noisy background in the case of as-grown samples (Fig. 6), but statements concerning the concentration change induced by the DH treatment cannot be given due to an upper limit of 1.5×10^{13} cm^{-3} (due to the background). From the admittance data, we obtained an activation energy of about 380 meV for ζ. Note that in co-evaporated CuInSe$_2$-based cells, the defect state ζ, also referred to as N2, is present with high concentration already in the as-grown state, such that it can easily be detected using admittance spectroscopy [27]. In that cell type, its concentration is proportional to the time elapsed under DH conditions [14].

For all samples, we estimate the Q-factor [37] (i.e., a measure for the influence of the series resistance on the DLTS spectra) to be much smaller than unity: the DLTS signals of as-grown and DH treated samples are not inverted. The temperature-dependent emission rates of the four different defect states (including the interface defect state θ) are displayed in the Arrhenius plot, Figure 8. For the recombination center ε, only the majority-carrier response is presented.

4. Numerical Simulations

We have performed calculations of the possible loss factors prominent in DH treated Cu(In,Ga)(S,Se)$_2$-based solar cells, taking advantage of the one-dimensional device simulation programme SCAPS [23, 38]. Details of the simulation parameters used can be found in preliminary studies [15], where we used the simplified heterostructure n-ZnO/CdS/Cu(In,Ga)(S,Se)$_2$, neglecting the i-ZnO layer. In this paper we take into account the i-ZnO layer with two alternative doping densities, 10^{15} cm^{-3} and 10^{18} cm^{-3} (in the following also denoted as low and high i-ZnO doping). Niemegeers et al. [23] used a relatively high doping concentration of 10^{18} cm^{-3} for their calculations. However, we determined the sheet resistance of i-ZnO on glass to be at least seven orders of magnitude larger than n-ZnO

on glass. Since we cannot obtain the doping density of i-ZnO in the completed heterostructure, we verify the numerical simulations by using the value 10^{15} cm^{-3} alternatively. We enclose only qualitative descriptions of the numerical simulations, i.e., trends, and point out that the significance of the numerical simulations is limited by the estimation of many unknown parameters for the present material system.

The crucial question whether the recombination at the buffer/absorber interface or in the bulk of the chalcopyrite layer plays a dominant role cannot be answered directly. The method of extrapolating the open-circuit voltage to $T = 0$ K, applied in earlier publications [14, 15] in order to determine the major recombination path, yielded the absorber bandgap energy, thus, in principle, indicating predominant recombination in the space charge region. For verification, we used SCAPS to calculate the temperature-dependent open-circuit voltages for two hypothetical sample definitions, one with bulk traps only, and the other with only interface defect states (uniform energy distribution). In both cases, the extrapolation of the open-circuit voltage to $T = 0$ K approximates the bandgap energy of the absorber. We conclude that this method of extrapolating the open-circuit voltage does not help in determining the major recombination path in the solar cell type investigated.

Furthermore, we looked at the influence of doping densities and concentrations of bulk and interface defect states on the open-circuit voltage and the band bending, in order to gain information on the potential major loss factors. Both parameters are available experimentally, the latter being proportional to the activation energy of the defect state β. After 438 h of DH exposure, we observed close to 20% loss of the open-circuit voltage V_{oc} (see Fig. 2) and a shift in the activation energy ΔE of β from about 50 meV to about 300 meV (see Figure 4). Using SCAPS, we computed which modifications of the sample parameters lead to electrical changes of a similar scale. A reduction of the n-ZnO and i-ZnO doping densities by three orders of magnitude can account for about a fifth of the V_{oc} loss and a clear increase of ΔE if the i-ZnO doping density is high. For low i-ZnO doping, both parameters vary only minimally. A concentration of interface defect states diminished by two orders of magnitude, however, changes ΔE drastically if the i-ZnO doping density is low; for the case of high i-ZnO doping, the changes happen on a much smaller scale. The open-circuit voltage is not influenced by the concentration of interface defect states. If both, the doping density of the window layers and the concentration of interface states, are reduced, then a major shift of ΔE of the order of the experimentally observed values becomes evident. A halved doping density of the absorber layer leads to a small reduction of V_{oc} and ΔE, accounting for a fifth to a tenth of the changes. A high concentration of bulk defect states has the largest impact on the open-circuit voltage. ΔE increases slightly for the case of acceptor-like defect states, but remains unaffected for recombination centers. Summarizing the results of our numerical simulations, the large shift of β can be mainly attributed to a decreasing concentration of interface states together with a diminishing doping density of the window layer. The increasing concentration of bulk defect states is the major contributor to the degradation of the open-circuit voltage.

5. Discussion

All layers of the Cu(In,Ga)(S,Se)$_2$ based heterostructure cells contribute to the DH induced changes of the fill factor and open-circuit voltage. We discuss the different layers successively, also giving account of the findings of other authors.

5.1. Window Layer

The front electrode commonly consists of an n-ZnO layer, an undoped i-ZnO layer, and a CdS buffer layer, the latter being in direct contact with the absorber. Experimental analysis of the surface morphology of DH tested Cu(In,Ga)Se$_2$ based heterostructure cells unveils some deterioration of the window layer due to microdefects of sizes ranging from 5 to 40 μm, which are located directly at the surface [39]. The DH exposure of ZnO layers on glass or Si substrates has been demonstrated to result in an increasing sheet resistance [9, 12, 13]. The degree of degradation is enhanced by the CdS layer located between ZnO and substrate, and is proportional to the thickness of the CdS layer [12, 13]. The increase in sheet resistance observed after 1000 h DH testing is found to be in the range between two and three. Wennerberg et al. [12] attribute these changes to a decreasing carrier concentration in the ZnO layers and state that it can account for only a small fraction of the fill factor losses. For modules, usually produced without a metal grid deposited on top of the window layer, the increase in sheet re-

sistance has a considerably larger effect on the overall performance [40].

Our own findings verify the results of Wennerberg et al. [12] for laboratory-scale samples: comparing test cells that were DH treated as complete device with the sets of samples where the process sequence was interrupted for a DH exposure after the absorber RTP, the CdS deposition, or the i-ZnO sputter process, respectively, we find out that the degradation of the window layer can be made responsible only for a small share of the total power loss [16].

5.2. Window/Absorber Interface

Lang et al. [41] point out that the surface of the absorber does not have the form of just a monolayer of atoms, but rather represents a transition region to the bulk semiconductor. Taking advantage of capacitance spectroscopy and DLTS, it seems to be impossible to distinguish whether a certain kind of defect is located directly at the surface layer or inside a thin interface region. Such a problem remains unsolved for the origin of the defect state β found in CuInSe$_2$ based solar cells, where the existence of an ordered vacancy or defect compound (OVC/ODC) of a few nanometers thickness has been reported [23].

Our capacitance spectroscopy measurements clearly show that the electrical properties of the interface region are modified by heat and humidity treatment. However, the shift of the interface defect state β, observed after DH exposure [14, 15, 18] and air annealing [27], does not only stem from changes of the interface, but is also influenced by the window and absorber bulk regions (doping concentration, defect state concentration) as well. Consequently, the band bending of the heterojunction and the type inversion at the absorber surface are diminished. Focussing on the results for the interface, we find that the Fermi-level pinning of as-grown cells is lifted for the case of complete devices [15], but remains unchanged when only the absorber layer was exposed to DH and the window layer deposited afterwards [16].

The defect state θ, being observed after the DH treatment (see Fig. 5), is probably located at the window/buffer interface or an internal grain boundary. We were not able to verify the spatial location and, thus, cannot judge the relevance of this defect state for the electrical changes of the DH treated samples.

Chemical modifications of the interface region due to heat and humidity have been observed as well.

Weinhardt et al. [42] have performed photoemission and X-ray emission spectroscopy experiments on Cu(In,Ga)(S,Se)$_2$-based heterostructures. They report on a DH induced oxidation of S atoms at the ZnO/CdS interface or at the ZnO/Cu(In,Ga)(S,Se)$_2$ interface, but do not observe oxidation at the CdS/Cu(In,Ga)(S,Se)$_2$ interface. Karg et al. [9] point out that the oxygen content of the cells, normally about one per mille of the amount of CuInSe$_2$, increases up to one order of magnitude due to DH exposure. The oxygen accumulates particularly at the buffer/absorber interface and the absorber/Mo interface. Such an effect is reported to be most pronounced for the case of Na doped films.

On basis of the current data, we cannot relate our electronic measurements to the observation of chemical modifications by other groups. The CdS/Cu(In,Ga)(S,Se)$_2$ interface region degrades due to the DH exposure and might be responsible for a fraction of the solar cell degradation, even though our numerical simulations do not suggest any influence on the degradation process. However, bear in mind that many simulation parameters are based on rough estimates only. We are not able to distinguish between a dominant recombination at the buffer/absorber interface or in the absorber bulk by experimental means.

5.3. Absorber Layer

Some of the bulk defect states detected in Cu(In,Ga)(S,Se)$_2$ based heterojunction cells are related to the DH induced degradation. We disclose the acceptor-like defect states ζ and γ, as well as the recombination center ε. The former can be observed after 144 h DH treatment, but is present in relatively low concentrations only. γ and ε can be clearly identified in as-grown samples, but are diminished due to the exposure to DH conditions. However, we believe that the concentrations determined are distorted by the influence of leakage currents [36] and by a superposition with another defect state in the case of γ. Additionally, the corresponding capacitance transients are non-exponential, making the standard method for evaluation of the defect concentration inaccurate [20]. This case usually takes place for high defect concentrations (order of a tenth of the doping density). Hence, we are not able to describe the DH induced changes of the defect spectra quantitatively.

Other groups have reported the observation of defect states related to the DH test as well. Schmidt et al. [14] measured an acceptor-like defect state called N2,

which is present in their as-grown co-evaporated samples in relatively high concentration, as it can be measured with admittance spectroscopy. They correlated the concentration of this defect state (estimated with a calculation by Walter et al. [43] based on their admittance data) with the open-circuit voltage of their devices. N2 is presumably identical to our ζ, even though its significance for the electrical characteristics seems to be quite different. Igalson et al. [17] observed N2 and a donor-like defect state N3 only after the DH treatment using DLTS, but did not determine the defect concentrations. The defect state N3 has emission rates comparable to ε and might signify the minority-carrier signal of ε. However, a verification is not possible, and N3 can as well correspond to the donor-like defect state κ which we found in Cu(In,Ga)(S,Se)$_2$-based solar cells with stoichiometry-varied absorber layer [44].

A current-voltage hysteresis, observed only after DH exposure of heterojunction samples and Schottky contacts, indicates a trapping mechanism in the absorber layer, i.e., an increasing concentration of deep traps. Also, within the numerical simulations, only an increasing concentration of deep defect states in the absorber layer can account for a major fraction of the losses of the open-circuit voltage. A decreasing absorber doping density due to DH exposure is equivalent to a reduced compensation, i.e., a net decrease of acceptor states – which, of course, can be achieved by an increasing concentration of donor-like states as well. However, the experimentally observed decreasing concentration of acceptor-like defect states can lead to a reduced compensation, but cannot account for the hysteresis. Thus, the detailed changes of the deep traps due to the DH treatment as well as the resulting electronic modifications are still unresolved.

Let us discuss the relation of the DH exposure and air annealing (oxygenation [6, 7]) phenomena to each other. The experimental difference is that DH testing is performed at a relatively low temperature (85 °C) combined with humidity treatment, whereas air (or oxygen) annealing happens at temperatures of above 200 °C without being subject to water vapor. The two major effects of oxygenation are a passivation of Se vacancies at the CdS/chalcopyrite interface and Cu migration into the absorber bulk [7]. We emphasize that both explanations are model pictures proposed to capture various experimental findings, but have been observed directly neither for air annealing nor for DH treatment. However, oxygen might play an important role

for the effects of DH exposure, as the amount of oxygen present in Na containing absorber layers increases by about one order of magnitude due to accelerated lifetime tests [9]. The similar results of the DH and annealing experiments, i.e., the shift of the interface defect state β and a decreased net doping density of the absorber, indicate a common origin for some of the underlying modifications, even though the correlation of the chemical changes with the electronic properties is unclear yet.

5.4. Back Contact

The Mo back contact undergoes an oxidation process due to DH exposure [12], but such degradation becomes electrically significant only if the module interconnections are destroyed [13]. Our electrical measurements indicate that there exists no additional electronic barrier evolving due to the DH treatment of complete heterostructure samples with durations of up to 438 h, i.e., the interface between the bulk absorber and the back contact remains ohmic.

6. Conclusions

The electronic effects of the damp-heat treatment at 85 °C ambient temperature and 85% relative humidity on ZnO/CdS/Cu(In,Ga)(S,Se)$_2$/Mo heterojunction solar cells have been investigated using current-voltage and capacitance-voltage measurements, admittance spectroscopy, and deep-level transient spectroscopy. We observed a reduced net doping density in the chalcopyrite absorber layer. Three absorber bulk traps with non-exponential capacitance transients were detected, two acceptor-like defect states and a recombination center. We were not able to determine the absolute trap concentrations, but expect superposition effects and the influence of leakage currents to be responsible for distorted capacitance transient amplitudes. However, the observation of a hysteresis in the current-voltage characteristics of damp-heat treated heterojunctions and Schottky contacts indicates an increased concentration of traps in the absorber layer. The Fermi-level pinning at the buffer/chalcopyrite interface, maintaining a high band bending in as-grown cells, is lifted due to the damp-heat exposure. The sheet resistance of the window layer increases. The combination of these effects leads to a reduction of the band bending and a diminished open-circuit voltage in the damp-heat treated solar cells.

[1] M. A. Contreras, B. Egaas, K. Ramanathan, J. Hiltner, A. Swartzlander, F. Hasoon, and R. Noufi, Prog. Photovolt. **7**, 311 (1999).

[2] V. Probst, W. Stetter, W. Riedl, H. Vogt, M. Wendl, H. Calwer, S. Zweigart, K.-D. Ufert, B. Freienstein, H. Cerva, and F. H. Karg, Thin Solid Films **387**, 262 (2001).

[3] J. Palm, V. Probst, R. Tölle, T. P. Niesen, S. Visbeck, O. Hernandez, M. Wendl, H. Vogt, H. Calwer, B. Freienstein, and F. H. Karg, Thin Solid Films (2002), in press.

[4] M. Powalla and B. Dimmler, in Proc. 29th IEEE Photovolt. Spec. Conf., edited by T. Anderson, IEEE, New York 2002, in press.

[5] U. Rau and H. W. Schock, Appl. Phys. A **69**, 131 (1999).

[6] D. Cahen and R. Noufi, Sol. Cells **30**, 53 (1991).

[7] U. Rau, D. Braunger, R. Herberholz, H. W. Schock, J.-F. Guillemoles, L. Kronik, and D. Cahen, J. Appl. Phys. **86**, 497 (1999).

[8] J.-F. Guillemoles, L. Kronik, D. Cahen, U. Rau, A. Jasenek, and H.-W. Schock, J. Phys. Chem. B **104**, 4849 (2000).

[9] F. Karg, H. Calwer, J. Rimmasch, V. Probst, W. Riedl, W. Stetter, H. Vogt, and M. Lampert, in Proc. 11th Int. Conf. on Ternary and Multinary Compounds, edited by R. D. Tomlinson, A. E. Hill, and R. D. Pilkington, Institute of Physics, Bristol 1998, p. 909.

[10] D. E. Tarrant and R. R. Gay, Final Tech. Report, 9/1995 – 12/1998, NREL (1999).

[11] D. E. Tarrant, A. R. Ramos, D. R. Willett, and R. R. Gay, in Proc. 21st IEEE Photovolt. Spec.Conf. (1990), p. 553.

[12] J. Wennerberg, J. Kessler, M. Bodegård, and L. Stolt, in Proc. 2nd World Conf. Photovolt., edited by J. Schmid, H. A. Ossenbrink, P. Helm, H. Ehmann, and E. D. Dunlop, European Comission, Brussels 1998, p. 116.

[13] M. Powalla and B. Dimmler, Thin Solid Films **387**, 251 (2001).

[14] M. Schmidt, D. Braunger, R. Schäffler, H. W. Schock, and U. Rau, Thin Solid Films **361/362**, 283 (2000).

[15] C. Deibel, V. Dyakonov, J. Parisi, J. Palm, S. Zweigart, and F. Karg, Thin Solid Films **403/404**, 325 (2002).

[16] C. Deibel, V. Dyakonov, J. Parisi, J. Palm, S. Zweigart, and F. Karg, in Proc. 17th European Photovolt. Solar Energy Conf., edited by B. McNelis, W. Palz, H. A. Ossenbrink, and P. Helm, WIP, München 2002, p. 1229.

[17] M. Igalson, M. Wimbor, and J. Wennerberg, Thin Solid Films **403/404**, 302 (2002).

[18] C. Deibel, V. Dyakonov, J. Parisi, J. Palm, and F. Karg, in Proc. 29th IEEE Photovolt. Spec. Conf., IEEE, New York 2002, in press.

[19] D. L. Losee, J. Appl. Phys. **46**, 2204 (1975).

[20] D. V. Lang, J. Appl. Phys. **45**, 3023 (1974).

[21] M. Schmitt, U. Rau, and J. Parisi, Phys. Rev. B **61**, 16052 (2000).

[22] M. Burgelman, F. Engelhardt, J. F. Guillemoles, R. Herberholz, M. Igalson, R. Klenk, M. Lampert, T. Meyer, V. Nadenau, A. Niemegeers, J. Parisi, U. Rau, H. W. Schock, M. Schmitt, O. Seifert, T. Walter, and S. Zott, Prog. Photovolt. **5**, 121 (1997).

[23] A. Niemegeers, M. Burgelman, R. Herberholz, U. Rau, D. Hariskos, and H. W. Schock, Prog. Photovolt. **6**, 407 (1998).

[24] G. P. Li and K. L. Wang, J. Appl. Phys. **57**, 1016 (1985).

[25] L. Dobaczewski, P. Kaczor, I. D. Hawkins, and A. R. Peaker, J. Appl. Phys. **76**, 194 (1994).

[26] S. B. Zhang, S.-H. Wei, A. Zunger, and H. Katayama-Yoshida, Phys. Rev. B **57**, 9642 (1998).

[27] R. Herberholz, M. Igalson, and H. W. Schock, J. Appl. Phys. **83**, 318 (1998).

[28] D. V. Lang, H. G. Grimmeiss, E. Meijer, and M. Jaros, Phys. Rev. B **22**, 3917 (1980).

[29] A. Niemegeers and M. Burgelman, J. Appl. Phys. **81**, 2881 (1997).

[30] R. Herberholz, T. Walter, C. Müller, T. Friedlmeier, and H. W. Schock, Appl. Phys. Lett. **69**, 2888 (1996).

[31] A. Yelon, B. Movaghar, and H. M. Branz, Phys. Rev. B **46**, 12244 (1992).

[32] L. Stolt and K. Bohlin, Solid-State Electron. **28**, 1215 (1985).

[33] D. B. Jackson and C. T. Sah, J. Appl. Phys. **58**, 1270 (1985).

[34] F. D. Auret and M. Nel, J. Appl. Phys. **61**, 2546 (1987).

[35] D. Schmid, M. Ruckh, and H. W. Schock, Sol. Ener. Mat. Sol. Cells **41/42**, 281 (1996).

[36] M. D. Chen, D. V. Lang, W. C. Dautremont-Smith, A. M. Sergent, and J. P. Harbison, Appl. Phys. Lett. **44**, 790 (1984).

[37] N. Fourches, Appl. Phys. Lett. **58**, 364 (1991).

[38] M. Burgelman, P. Nollet, and S. Degrave, Thin Solid Films **361/362**, 527 (2000).

[39] G. A. Medvedkin, E. I. Terukov, Y. Hasegawa, K. Hirose, and K. Sato, Sol. Ener. Mat. Sol. Cells (2002), in press.

[40] J. Wennerberg, J. Kessler, and L. Stolt, Sol. Ener. Mat. Sol. Cells (2002), in press.

[41] D. V. Lang, J. D. Cohen, and J. P. Harbison, Phys. Rev. B **25**, 5285 (1982).

[42] L. Weinhardt, M. Morkel, T. Gleim, S. Zweigart, T. P. Niesen, F. Karg, C. Heske, and E. Umbach, in Proc. 17th European Photovolt. Solar Energy Conf., edited by B. McNelis, W. Palz, H. A. Ossenbrink, and P. Helm, WIP, Müunchen 2002, p. 1261.

[43] T. Walter, R. Herberholz, C. Müller, and H. W. Schock, J. Appl. Phys. **80**, 4411 (1996).

[44] C. Deibel, A. Wessel, V. Dyakonov, J. Parisi, J. Palm, and F. Karg, Thin Solid Films **431/432**, 163 (2003).